Biointerface Research in Applied Chemistry
Open-Access Journal (ISSN: 2069-5837)

Article
Volume 13, Issue 3, 2023, 286
https://doi.org/10.33263/BRIAC133.286

Design and Fabrication of pH-Sensitive Curcumin Coated Gold Nanorods as Anti-Angiogenic Targeting Nanostructures

Rathi Usha Kannan [1], Geeva [1], Suresh Sethurajan [2], Shoba Narayan [1,*]

[1] Faculty of Allied Health Sciences, Chettinad Hospital and Research Institute, Chettinad Academy of Research and Education, Kelambakkam, Chengalpattu District, Chennai Tamilnadu, 603103, India
[2] CATERS, CSIR-Central Leather Research Institute, Adyar, Chennai, 600020, India
* Correspondence: shobulu@gmail.com; shobanarayan@care.edu.in (S.N.);

Scopus Author ID 10142117400
Received: 12.03.2022; Accepted: 29.04.2022; Published: 10.07.2022

Abstract: Curcumin's limited bioavailability, caused by its hydrophobic nature, is a significant stumbling block to its application. This paper describes the development of a pH-responsive targetable carrier that overcomes the challenges associated with using curcumin. The use of gold nanorods in the creation of curcumin nanocarriers aids the combination of plasmonic phototherapy with biotherapy. This study used the pH-sensitive release and receptor targeting nanocarriers poly-L-histidine and ATWLPPR. The carrier's components are confirmed through synthesis and characterization. At a concentration of 0.66 μg/mL), the functionalized gold nanorod nanocarrier had a 32 - 43 nm size range. The gold nanorod level is increased to 1.33 μg/mL by crosslinking them with amine-functionalized PEG. Curcumin was released in a pH-dependent manner by the nanocarrier. Furthermore, in vitro tests to corroborate the efficiency of this therapeutic model show that when gold nanorods are routed through the peptide, the intake of gold nanorods is doubled.

Keywords: gold nanorods; pH-sensitive polymer; multifunctional therapeutics; cellular uptake; targeted drug delivery; peptide.

1. Introduction

For decades cancer-based treatment regimens such as chemotherapy, radiation, immunotherapy, and hormonal therapies have failed to treat cancer due to their increased risk of damage caused to the healthy cells and inferior methods of eradicating cancerous cells. Nanotechnology-based theranostic drug delivery agents are poised to play a leading role in cancer therapy [1]. Theranostics include imaging, drug loading, sustained and targeted release, higher in vivo circulation times, and a large surface that is active enough for modifications [2,3]. Iron oxide nanoparticles, gold nanoparticles, silver nanoparticles, liposomes, polymeric nanoparticles, and nano-emulsions form multifunctional therapeutic strategies for cancer treatment [4,5]. Salient features that make gold nanoparticles ideal for imaging, therapeutics, drug, and gene delivery are a) low toxicity, b) ease of attaining different sizes and shapes, c) functionalization with a variety of molecules, d) range of optical and chemical properties, e) absorption and f) scattering of light [6,7]. Though several morphological forms of gold nanoparticles exist, Gold nanorods (GNRs) with a higher plasmonic photothermal therapeutic and binding efficiency have the edge over other nanoforms of gold as a drug delivery agent [8].

The interaction between the external light source and the nanorods through the biological tissue improves by using nanorods that can have their plasmon resonance shifted in the near-infrared region [9]. Usefulness in bioimaging applications enhances by varying the aspect ratio, i.e., length to width of the nanorods, as it changes the wavelength of absorption and scattering [10].

Curcumin is a polyphenolic compound having a diferuloylmethane structure. It is extracted from turmeric (Curcuma longa), a medicinal plant with anticancer properties [11]. This compound is non-toxic and can affect growth factor receptors and cell adhesion molecules in tumor growth [12]. Research studies show that 12 g of curcumin per day is safe and effective for treating lung, pancreatic, colorectal, breast, head, and neck cancer. The use of curcumin for anticancer activity is relevant as it promotes anti-proliferative, anti-invasive, antiangiogenic, and apoptotic activities, both in vitro and in vivo [13,14]. Formulation of curcumin as liposomes, micelles, metal, polymeric nanoparticles, and emulsions is essential to overcome the limitations in use, such as low water solubility and thus low bioavailability [15].

Herein we developed curcumin-coated gold nanorods with modified surface chemistry for further biomedical applications. For instance, PEG helps to overcome the insignificant pharmacokinetic properties often encountered in traditional drug delivery methods. The enhanced permeation and retention (EPR) effect is crucial for an ideal drug delivery system [16]. The PEG conjugated drug delivery system has better EPR effects compared to other drug delivery systems [17] and is highly inert toward bio-molecular interactions. Improvement in therapeutic efficiency is obtained through a) increased hydrophilicity, b) improved stability, c) controlled release, d) non-immunogenic character, e) prolonged drug half-life, and f) enhanced pharmacokinetic and pharmacodynamic profiles [18].

This work hypothesizes that gold nanorods conjugated with PEG would have reduced reticuloendothelial system-based non-specific uptake based on the literature in this area. PEG conjugation would thus help passive tumor targeting and enhance permeability and retention in solid tumors. To achieve controlled and pH-sensitive drug release, coating with polymers such as poly(amido amines), carboxymethyl chitosan, and poly (L-histidine) is reported [19]. This study employed poly (L-histidine) to achieve pH-sensitive drug release. A hydrazine linkage in poly (L-histidine) can lead to drug release through protonation of the imidazole ring. Poly (L-histidine) improves hydrophilicity and membrane fusion at endosomal pH [20].

Tumor angiogenesis, the proliferation of new blood vessels from pre-existing vessels, is a unique feature of tumor formation and involves growth factors such as the vascular endothelial growth factor – 165 (VEGF165). Neuropilin 1(NRP-1) and co-receptor of NRP-1 have been identified as regulators for neural development and non-tyrosine kinase receptor for VEGF165, respectively. The co-expression of VEGFR-2 and NRP-1 increases the binding of VEGF165 to VEGFR-2 and enhances VEGF165 mediated signaling. NRP-1 is overexpressed in the microenvironment and constitutes malignant tumor development [21,22].

Drug targeting through peptides specific to overexpressed receptors or co-factors during a tumor reduces side effects. A low molecular weight heptapeptide, ATWLPPR peptide, can selectively bind to the NRP-1 receptor [23]. Peptide modification, such as in liposomal paclitaxel, is reported to have improved the antiangiogenic properties [24].

This manuscript reports an improvement in the efficacy of curcumin, a known anticancer drug [25], through a nanocarrier comprising PEG conjugated gold nanorods carrying poly (L-histidine) for pH-sensitive release of curcumin and carrying an NRP-1 targeting peptide ATWLPPR through thiol conjugation. The study has gained an understanding of in

vitro cytotoxicity, antiangiogenic properties, cellular uptake, and distribution on NRP-1 expressing HUVEC cells.

2. Materials and Methods

2.1. Materials/Chemicals.

All major chemicals procured were of analytical grade and purchased from Sigma Aldrich Co, St. Louis, USA. The chemicals included Gold chloride, Cetyl trimethyl ammonium bromide, Sodium borohydride, PEG-diamine, Silver nitrate, Ascorbic acid, and Curcumin, Polyethylene glycol, Poly- L-Histidine, 1-Ethyl-3-3-Dimethylaminopropyl Carbodiimide, and Dimethylformamide. VEGF inhibitor peptide was purchased from Merck, Germany. Other chemicals for this work were obtained from Sisco Research Laboratories, Chennai, India. And Hi-Media Laboratories Ltd., Chennai, India. HUVEC cells were sourced from Sigma Aldrich Co., and PC 12 Cells were obtained from National Centre for Cell Science, India. Milli-Q water was used to dissolve water-soluble chemicals.

2.2. Synthesis and functionalization of gold nanorods (G).

Peptide-tagged pH-sensitive polymer conjugated curcumin-coated gold nanorods were prepared by following the methodology presented in Scheme 1.

2.3. Preparation of curcumin (C) coated gold nanorods.

Standard methods were used throughout the study to prepare gold nanorods with slight modifications. The synthesis was carried out at room temperature in 5 mL leak-proof screw-capped vials. Au seed solutions and gold nanorods (GNRs-CTAB) stabilized using surfactant agents like cetyl trimethyl ammonium bromide were prepared by the already reported method [26]. The same approach was adopted to prepare 0.15 M, 0.2 M, and 0.25 M concentrations of CTAB-containing nanorods. The prepared gold nanorods were coated by modifying earlier methods [27,28]. Here, 0.1 mL of 2.7 mM (5 mg/5 mL ethanol) of curcumin solution was added to 4 mL of as-prepared gold nanorod solutions. And then, it was kept in a vial shaker for 6 hrs for complete mixing and centrifuged at 10,000 rpm for 10 mins. The pellet was redispersed by adding 4 mL of Milli Q water. The shaking in a vial shaker and centrifugation were followed in between each functionalization step.

2.4. Functionalization of PEG (Polyethylene glycol-P) on curcumin coated GNR followed by Peptide functionalization without bifunctional crosslinker and pH-sensitive peptide (GCP^{Pep}).

PEG coating is essential to improve the biocompatibility of nanoparticles. PEG coating and functionalization of prepared curcumin-coated gold nanorods were carried out by reported procedures [29-31] (Supplementary Information).

2.5. Conjugation of Peptide (pep) and PLH (Poly- L-Histidine) on PEG-diamine (NH2) tagged curcumin coated gold nanorods (GCP^{NH2pep}).

To covalently bind peptides to the pH-sensitive polymer, bioconjugation was adopted [32]. Here 0.05 mM of PEG-diamine in water was prepared at 50 ^{o}C, and then the next set of 0.025 mM of PLH solution in Dimethylformamide was made by following the earlier method [33]. After this, 0.05 mM of EDC solution was added. EDC activated the amine group of PEG-

diamine to the conjugate peptide on PEG-diamine, and the activation of *the* Carboxylic Group in PLH by EDC was done [34]. Dialysis was done for 2 hours against water under stirring conditions to remove the excess EDC. To conjugate PLH on NH_2-PEG-peptide, 3 mL of EDC activated PLH, and 2 mL of NH_2-PEG-peptide solution were taken in the dialysis membrane. It was dialyzed against deionized water under stirring for two hours to remove the excess EDC solution. For the functionalization of NH_2-PEG-peptide + PLH (P^{NH2Pep}) and NH_2-PEG-PLH on curcumin-coated gold nanorods, 4 mL of centrifuged curcumin-coated gold nanorods were taken in two 5 mL tubes and then 1 mL of NH_2-PEG-peptide (P^{NH2Pep}) + PLH and 1 ml of NH_2-PEG-PLH were added each tube respectively.

2.6. Characterization: DLS and Zeta potential.

The hydrodynamic diameter and the zeta potential of the prepared seed solutions, gold nanorods (G) with different concentrations of CTAB solutions, curcumin-coated gold nanorods (GC), PEG, and curcumin-coated gold nanorods (GCP), peptide-functionalized PEG and curcumin coated (GCPPep) were determined. Malvern Zetasizer was used to characterize gold nanorods. The following samples were prepared for the DLS measurements a) 1 mL of gold nanorods (G), b) 1 mL of curcumin-coated gold nanorods (GC), c) 1 mL of PEG and curcumin-coated gold nanorods (GCP), d) 1 mL of peptide-functionalized PEG (GCP^{Pep}) and Curcumin coated gold nanorods, e) 1 mL of NH_2-PEG-PLH functionalized curcumin coated gold nanorods with peptide (GCP^{NH2pep}), f) 1 mL of NH_2-PEG-PLH functionalized curcumin coated gold nanorods without peptide (GCP^{NH2}). The solutions were centrifuged at 10,000 rpm for 10 mins. The supernatant was discarded. Pellet obtained was redispersed with 1 mL of Milli Q water. Then the samples were characterized by DLS. The samples were used for the Zeta potential determination by adding 200 μL of Milli Q water to each sample.

The pH variability study was carried out with different pH buffer solutions (pH – 2.6, 4.1, 5.6, 6.1, 7, 8.9, and 10). For this, 0.2 mL of the centrifuged PEG and curcumin-coated GNR was added to 0.8 ml of different pH solutions and kept in a shaker for 2 hours. To understand the drug release [35] of curcumin from GCP^{Pep} and GCP^{NH2pep}, the solutions were placed at two different pHs, 7.4 and 5.5. This pH was chosen to know how the pH-sensitive polymer can open and help release drugs at that pH. The solutions were centrifuged after two hours, and the concentration of curcumin in the supernatant was determined by HPLC analysis.

2.7. Biophysical characterization of fabricated nanoparticles.

For the UV-Visible absorption spectra of the prepared samples, the baseline was set from 200 to 900 nm with 1 mL of Milli Q water. After baseline setting to understand the plasmonic bands [36], 0.5 mL of seed solution, G, GC, GCP, GCP^{Pep}, $GCP^{NH2pep,}$ and GCP^{NH2} were taken individually with 2.5 mL of Milli Q water and 1 mL was made in a cuvette and analyzed. Gold nanorods, curcumin coated gold nanorods, PEG and curcumin coated gold nanorods, peptide-functionalized PEG and curcumin coated gold nanorods, NH_2-PEG-PLH functionalized curcumin coated gold nanorods with and without peptide were characterized by infrared spectroscopy in the range of 650 - 4000 cm^{-1} to study about the stretching and bending vibration mode, intermolecular interactions that are present in those samples. The FTIR samples were prepared by following the above procedures except for the re-dispersion step. Then the pellets are lyophilized and used for the FTIR analysis.

The X-ray diffraction pattern was made to understand the crystallinity. Gold nanorods, curcumin-coated gold nanorods, PEG and curcumin-coated gold nanorods, peptide-functionalized PEG, and curcumin-coated gold nanorods, NH_2-PEG-PLH functionalized curcumin coated gold nanorods with and without peptide were analyzed using Miniflux II, Rigaku diffractometer with CuKα radiation (λ = 0.1548 nm). The operating scanning range was 5 to 80 degrees and a scan speed of 1^o min^{-1}. For this, the samples were prepared as same as FTIR sample preparation. To determine the exact size and morphology, the samples were characterized by TEM. All samples were centrifuged, washed and 5 mL of the sample was placed on the grid and analyzed using TEM

2.8. High-performance liquid chromatography studies.

HPLC analysis was done to determine the concentration of the drug (curcumin). In HPLC analysis, acetonitrile and methanol were used as a mobile phase with a flow rate of 1 mL/min. The volume used for the injection was 20 mL, and curcumin was analyzed at 424 nm wavelength. HPLC sample preparation: 10 µL, 15 µL, 25 µL, 35 µL, and 50 µL of curcumin solution (2.7 mM) were taken in a 2 ml tube, and the volume was made up to 1 mL using Milli Q water. Then these samples were used for further analysis with 4 ml of the supernatant of curcumin-coated gold nanorods solution. This 4 ml supernatant was used as an unknown sample. Samples with known concentrations were run, and the plot of retention time versus concentration was plotted to determine the unknown concentration. Measurements were carried out in duplicates.

2.9. Inductively coupled plasma-optical emission spectroscopy.

To determine the concentration of gold that is present in the following samples, gold nanorods curcumin coated gold nanorods, PEG and curcumin coated gold nanorods (GCP), peptide-functionalized PEG and curcumin coated GNR (GCP^{Pep}), NH_2- PEG-PLH functionalized curcumin coated gold nanorods with peptide (GCP^{NH2Pep}) and without peptide (GCP^{NH2}). The samples were prepared the same as the above procedure up to the centrifugation step. From the centrifuged sample, 1 mL of supernatant was separately mixed with 100 ml of aqua regia and 5 mL of water and further used for ICP-OES analysis.

2.10. Differential scanning calorimetry analysis.

The thermal stability of all samples was determined by DSC (Q200, TA Instruments) and scanned over a range of -90.06 to 396.70 ^oC at a heating rate of 19.99 ^oC per min in a nitrogen atmosphere. Here 2 mL of all the samples were taken, and the preparation procedure was followed the same as FTIR sample preparation.

2.11. Cellular uptake studies in PC 12 cells.

Cells (PC12) were cultured in a T25 flask using DMEM medium supplemented by 10 % (v/v) FBS. Antibiotics penicillin (100 U/mL), and streptomycin (100 mg/mL) were also added. Cells were incubated (humidified and controlled atmosphere with a 95 % to 5 % ratio of air/CO_2, at 37 °C). The confluent cells were split using 1X trypsin. These confluent cells were used for cellular uptake studies [33]. The cultured PC 12 cells were centrifuged at 1300 rpm for 10 mins and supplemented by the same medium. The cellular uptake studies of gold nanorods were carried out in 6 well plates. The 3 µg of gold-containing G pellet, GC pellet,

GCP pellet, GCP^{Pep} pellet, GCP^{NH_2}, GCP^{NH_2Pep} were added with 500 µL of DMEM medium in a 2 ml tube. Then it was seeded into the six-well plates through a syringe filter. After that, the DMEM supplemented cultured PC 12 cells 500 µL were seeded into the wells of the plate. Then it was kept in an incubator for 2 hours. After 2 hours, the solution from the wells was transferred into the 2 mL tube and centrifuged (10,000 rpm for 10 mins). The supernatant was taken and transferred into a new tube and mixed with 50 µL of aqua regia. Then it was further analyzed by ICP-OES analysis.

2.12. Cellular uptake of gold nanorods in HUVEC cells and tube formation assay.

HUVEC (Cat NO: 200 P-05n) were cultured using endothelial growth medium (Cat NO: 211-500) in an incubator at 37.8 ^oC in the presence of 5 % CO_2 and 95 % relative humidity. The medium was replenished every two days. On reaching 90 % confluency, cells were harvested by trypsinization. Cellular uptake studies were done by seeding HUVEC cells on 96 well plates at 200 µl per well in Dulbecco's Modified Eagles Medium. Then the cells were treated with 3 µg of gold-containing G, GC, GCP, GCP^{Pep}, $GCP^{NH2,}$ and GCP^{NH2Pep} and were dispersed in 1 ml of Dulbecco's Modified Eagles Medium and filtered in a syringe filter to avoid contamination and the solution was then added to cells. The cells were incubated for two hours and monitored under a microscope. The tube formation assay was carried out by preparation of extracellular matrix gel (ECM) and 1X staining buffer.

The ECM gel was prepared by thawing overnight on the ice at 4^oC. The 50 µl of thawed ECM gel was added to each of the pre-chilled 96-well-sterile plates. The ECM gel in the sterile plates is incubated at 37°C for 30 minutes for one hour. The endothelial cells are harvested in Dulbecco's Modified Eagles Medium containing 0.5 %-10 % serum. The cell suspension containing 150 µL of approximately 1.5-3 x 10^4 cells was added to the plates containing solidified ECM gel. The assay plates were incubated at 37 ^oC, for 4-18 h. The cells were observed using a light microscope at a high magnification field. The extent of tube formation was inspected by the length and branch points of the cells.

3. Results and Discussion

3.1. Synthesis of functionalized gold nanorods.

The study used gold nanorods synthesized from seed solutions prepared with varying concentrations of CTAB as a capping agent (0.1 - 0.25 M, in units of 0.05 M) and sodium borohydride as a reducing agent [37]. The optimization of CTAB concentration was critical as it influences the aspect ratio of the nanorods and thus the tuning of longitudinal plasmonic resonance to the near-infrared wavelength region [38-41].

UV-Vis spectroscopy, a simple tool, is widely employed to understand the changes in the plasmonic resonance band of gold nanorods. Figure I provides the UV-Vis spectrum of gold nanorods (G), curcumin-loaded nanorods (GC), and peptide-coated curcumin-loaded nanorods (GCP).

The C-terminal of the ATWLPPR peptide has a vital role in the binding of the peptide to PEG. Functionalization of the curcumin-loaded gold nanorods with poly(L-histidine) through a conjugation using amine-PEG and its subsequent attachment to ATWLPPR through EDC was studied. In this type of binding chemistry, the amine group of PNH2 binds with the carboxylic group of PLH. The PLH will link only with one side of the amine group that is

present in PNH2 due to the steric hindrance [42]. The unbound amine group of PNH2 is then conjugated using reported EDC conjugation chemistry to the C-terminal (LPPR) sequence of the ATWLPPR peptide [43]. This study employed thus prepared gold nanoconjugate (GCP^{NH2pep}). Figure 1 depicts the changes in the absorbance spectra of the conjugates with functionalization. For better clarity, Scheme 1 provides a schematic overview of the design of peptide-functionalized gold nanorods. This study has taken specific care to adopt conjugation strategies for poly (L-histidine) and ATWLPPR against conventional adsorption methods to ensure effective curcumin delivery to the NRP-1 in HUVEC cells.

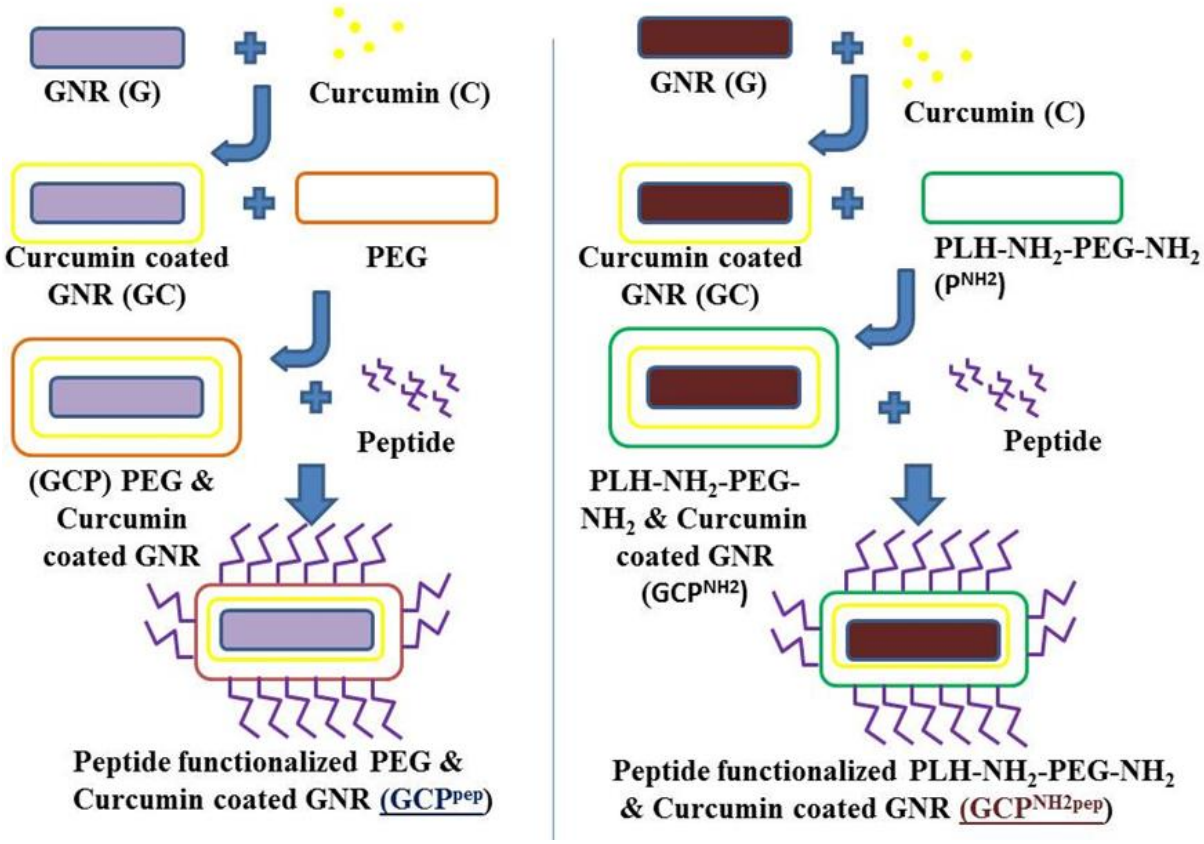

Scheme 1. Preparation scheme for peptide-tagged pH-sensitive polymer conjugated curcumin-coated gold nanorods.

3.2. UV-Visible spectroscopic studies.

Absorption spectra of all samples were recorded using a UV-Vis Spectrophotometer, in the 200 and 900 nm wavelength range, at every step of the experiment. For this, 0.5 ml of the prepared G, GC, GCP, GCP^{NH_2}, GCP^{Pep}, and GCP^{NH_2Pep} were mixed with 2.5 ml of Milli Q water and measured against Milli Q water and Ethanol as a reference. The seed solution with different concentrations of CTAB shows different λ_{max} that are in the visible range (Figure S1, Supplementary Information). The G solutions with varying levels of seed solutions also show different λ_{max} in transverse peaks nearly at the visible region and longitudinal peaks in the near-infra-red region (Figure S2, Supplementary Information). 0.15 M CTAB is the optimal concentration based on the absorption of G. CTAB containing G solutions have higher intensity in the longitudinal absorption peak position with λ_{max} at 743 nm than the transverse peak with λ max at 525 nm at 0.15 M. The peaks fall in the visible – IR region. Strong absorption of near-infrared light provides for deep penetration into the tissues, which has been the basis for employing G in the photothermal therapy of tumor cells [44]. No significant difference in the UV-Vis spectra of the products was observed before and after centrifugation (Figure 1C and

1D) of G, GC, and GCP. Any small change observed is attributed to the difference in the refractive index. An increase in the intensity of the transverse absorbance peak of GCP^{Pep}, GCP^{NH_2}, and GCP^{NH_2Pep} compared to the longitudinal peak is attributable to the higher binding of the peptide in the longitudinal band (Figure 1E – IF).

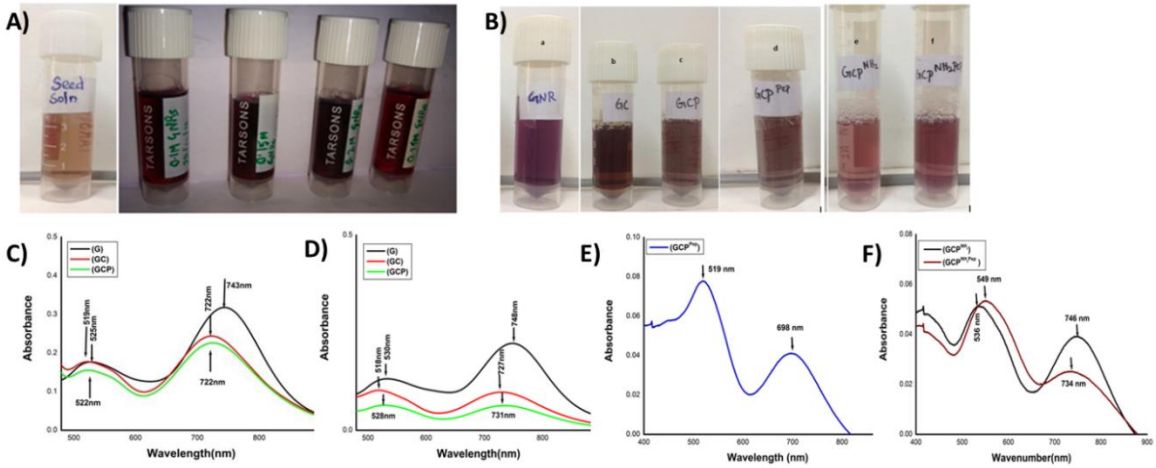

Figure 1. (**A**) Photograph of seed solution and gold nanorods prepared using different concentrations of CTAB (left to right); (**B**) Photograph of synthesized nanorods and functionalized nanorods using bioconjugation chemistry (**a**) G, (**b**) GC, (**c**) GCP, (**d**) GCP^{Pep}, (**e**) GCP^{NH2}, (**f**) GCP^{NH2Pep}; (**C**) UV-Visible absorption spectrum of G, C coated G, P and C coated GNR before centrifugation; (**D**) UV-Visible absorption spectrum of G, C coated G, P and C coated G after centrifugation; (**E**) UV-Visible absorption spectrum of peptide-functionalized, P and C coated GNR; (**F**) UV-Visible Spectrum of P^{NH2} functionalized C coated G and P^{NH2Pep} functionalized C coated G;

3.3. Morphological studies by TEM.

The morphology of prepared gold nanorods was evaluated through transmission electron microscopy. The resultant images demonstrate the morphology as rod-shaped (Figure 2). From the figures, it can be seen that functionalization did not change the shape of the nanorods, and the size of the rods was around 30 nm. Earlier studies have also indicated intact morphology of gold nanorods is very important for therapeutic applications [45,46]. Previous studies showed that peptides isolated from phage biopanning on conjugation to gold nanorods did not change the photothermal property of gold nanorods [47]. From the UV Vis absorbance spectroscopy, peptides bound to PEG without crosslinking showed a blue shift in absorbance. The blue shift was shifted to the NIR region when the peptide was conjugated through a bifunctional crosslinker. Similarly, an aggregation of gold nanorods is observed under TEM (Figure 2D). The same was not found when the nanorods were conjugated to the peptide through the bifunctional crosslinker (Figures 2E and 2F).

3.4. DLS and Zeta potential measurements.

Figures 3 A to F represent the size distribution of gold nanorods and functionalized nanorods. The corresponding hydrodynamic diameter and zeta potential are presented. The hydrodynamic diameter of G was found to be 42 nm, with a zeta potential of +51.3 mV. The charge of the prepared rods can be attributed to the presence of positive charged CTAB on the surface of G. With the coating of C on G, and there is a reduction in size to 32.64 nm with a zeta potential of + 11.2 mV. The results are in expected lines as CTAB will be replaced by curcumin. Subsequent coating of PEG on GC resulted in a marginal increase in size to 37.84 nm, with a zeta potential value of + 26.6 mV. This observation is further substantiated by TEM.

In the case of amine-functionalized PEG-PLH conjugated GC, the size was found to be 38 nm with a zeta potential +25.7 mV (Figure 3).

Here the PLH and P^{NH2} could have played a role in preventing aggregation, as observed by other researchers [48]. The hydrodynamic diameter of nanoparticles is dependent upon the interface charge during physicochemical interactions [49]. It can be seen that there is no significant difference in hydrodynamic diameter of GCP and GCP^{NH_2} on the conjugation to the peptide. The increase in zeta potential values in both the conjugated peptide samples signifies the importance of electrostatic interaction in stabilizing nanoparticles [50], possibly due to the role of peptide and PEG and a small sequence of the peptide [51]. Nano-based drug delivery system, in reality, has to encounter various ions, proteins, charged molecules, etc., due to the physicochemical conditions of the biological system [52]. The samples were brought to variable pH conditions using phosphate-buffered solutions to understand the changes in hydrodynamic diameter and zeta potential. It can be seen that there is an increase in the hydrodynamic diameter of nanorods with a decrease in pH. Positive values for zeta potential were observed at pH 2.60, 4.05, and 5.60. When the samples cross the isoelectric point [53], the zeta potential is negative (at pH 6.13 and 7.02). The corresponding data is presented in Figure 4.

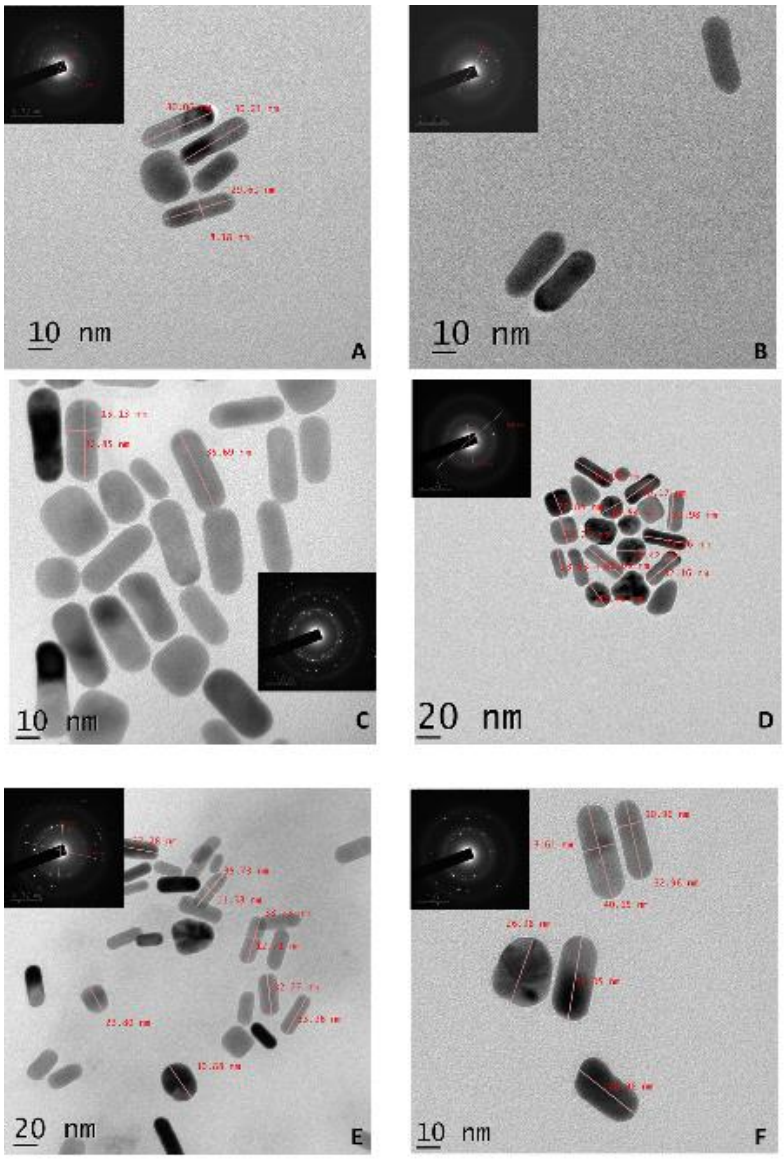

Figure 2. (**a**) TEM micrographs of (**A**) G, (**B**) GC, (**C**) GCP, (**D**) GCP^{Pep}, (**E**) GCP^{NH2}, (**F**) GCP^{NH2Pep}.

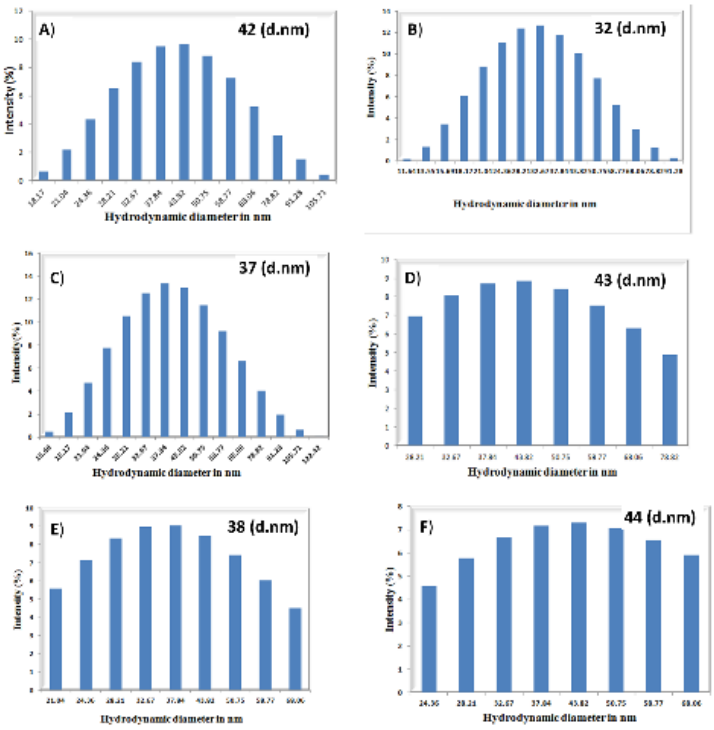

Samples	Average Hydrodynamic diameter in nm	Zeta potential (mV)
G (A)	42	+51.3
GC (B)	32	+11.2
GCP (C)	37	+26.6
GCP^{Pep} (D)	43	+24.9
GCP^{NH_2} (E)	38	+25.7
GCP^{NH_2Pep} (F)	44	+32.8

Figure 3. Hydrodynamic diameter and zeta potential measurements of synthesized and functionalized rods (**A**) G, (**B**) GC, (**C**) GCP, (**D**) GCP^{Pep}, (**E**) GCP^{NH2}, (**F**) GCP^{NH2Pep}.

3.5. FTIR analysis of binding of functionalities to gold nanorods.

One of the important tools to study the functional groups that are attached to the nanoparticle surface is FTIR [54]. Figure 4b shows the binding functionalities of gold nanorods with different chemicals. Due to the presence of methyl and methylene groups in CTAB and curcumin, the G, GC, and GCP have CH stretching vibrations at 2918 cm^{-1}, 2850 cm^{-1}, 2848 cm^{-1}, and 2850 cm^{-1}. Due to the presence of ascorbic acid, the aromatic vibrations were observed in G at 1660 cm^{-1} and 1445 cm^{-1}. Similarly, the presence of curcumin in GC and GCP could be seen from the aromatic vibrations at 1686 cm^{-1}, 1660 cm^{-1}, and 1631 cm^{-1}. C-O stretching and C-H bending vibrations were observed in G due to CTAB at 1100 cm^{-1}. In GC, GCP, the bending vibrations were observed at 1024 cm^{-1}, 1246 cm^{-1}, and 1103 cm^{-1} due to the presence of curcumin. The heptadiene bending vibrations were found at 1425 cm^{-1} and 1380 cm^{-1} due to the presence of curcumin in GC and GCP. The NH wagging vibration was noted in G and GC due to the presence of CTAB. Figure 4a shows that due to the presence of peptide and PLH the =CH stretching, -CH stretching vibrations, carboxylic bond , C-C stretch of aromatic ring and C-O stretching vibrations were observed at 2957 cm^{-1}, 2875 cm^{-1}, 1738 cm^{-1}, 1494 cm^{-1}, 1168 cm^{-1} in GCP^{Pep} at 2957 cm^{-1}, 2875 cm^{-1}, 1738 cm^{-1}, 1494 cm^{-1}, 1168 cm^{-1} in $GCP^{NH}{}_2$ at 2957 cm^{-1}, 2875 cm^{-1}, 1738 cm^{-1}, 1494 cm^{-1}, 1168 cm^{-1} in GCP^{NH2Pep}. The amide bonds, C-H deformation, and C=C stretches were absorbed in GCP^{NH2} and GCP^{NH2Pe}p due to the presence of amine-functionalized PEG. These changes in the vibrational bands confirmed the functionalization of different molecules of gold nanorods.

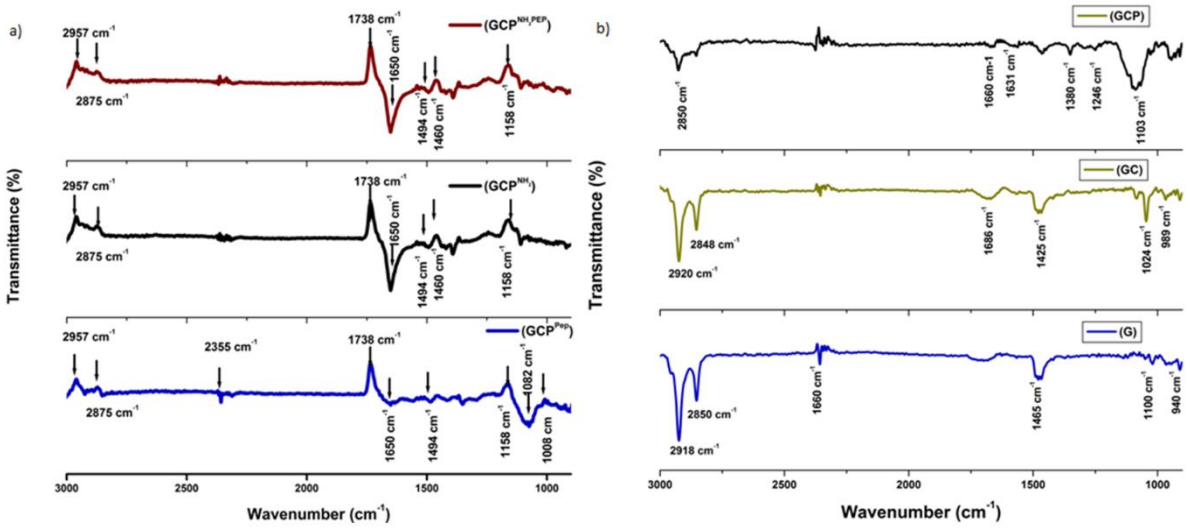

Figure 4. FT-IR spectrum of (**a**) functionalized and (**b**) synthesized rods.

3.6. XRD analysis of crystallinity changes with functionalization.

XRD analysis provides information about the crystalline structure of the particles binding functional groups to the nanoparticles through changes in the sharpness as well as the intensities of peaks [54]. The G and GC show the crystalline peaks with miller indices (110), (200), (220), and (311) (Figure 5a). However, GCP, GCP^{Pep}, GCP^{NH2}, GCP^{NH2Pep} show broad XRD peaks, and there is a reduction in peak intensity, indicating the presence of functionalities via PEG or peptide on the nanoparticle surface. It can also be observed that GCP, GCP^{Pep}, GCP^{NH2}, GCP^{NH2Pep} when compared with G and GC, show an amorphous nature [55] due to the presence of PEG and NH2-PEG-NH2 as shown in (Figure 5 a and b**)**.

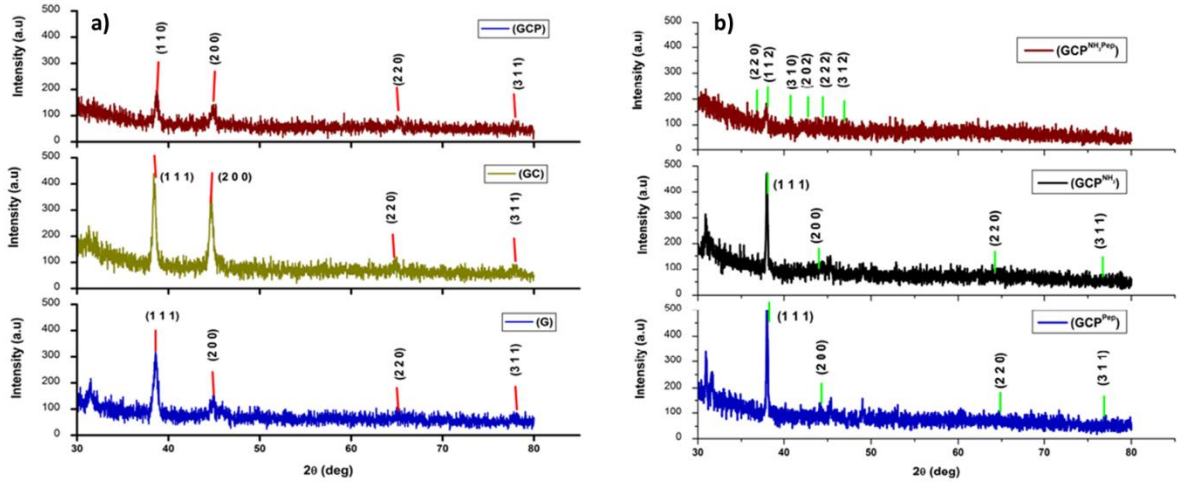

Figure 5 XRD spectra of (**a**) synthesized, (**b**) functionalized gold nanorods, and (**c**) standard XRD spectra of gold nanorods.

3.7. Determination of curcumin concentration and pH-sensitive polymer on drug release.

For further in vitro and in vivo studies, it is essential to know the amount of curcumin loaded in gold nanorods. The concentration of curcumin is determined by UV-Vis spectroscopy [56] or by the HPLC method [57]. HPLC method is a sensitive method for assessing the level of unknown analytes. In the HPLC method, the absorption of curcumin by gold nanorods and the release of curcumin at pH 7.4 and 5.5 was determined from a standard plot prepared in the curcumin concentration range of 10 µg/mL to 50 µg/mL. The retention

time of curcumin was about 5.36, and the λ max was 424 nm. From the standard plot of concentration versus the area under the peak, the percentage of curcumin loaded to the gold nanorods was 20.9 ± 1.5. PLH plays a vital role in ensuring drug release inside the cell, which is ideal under acidic pH conditions. To understand the pH-sensitive release of curcumin from GCP and GCP^{NH2Pep}, the nanocarriers incubated at pH 7.4 and 5.5 for two hours were employed. At pH 7.4, compared to GCP (0.1µg), GCP^{NH2pep} (0.21 µg) had a one-fold increase in curcumin release.

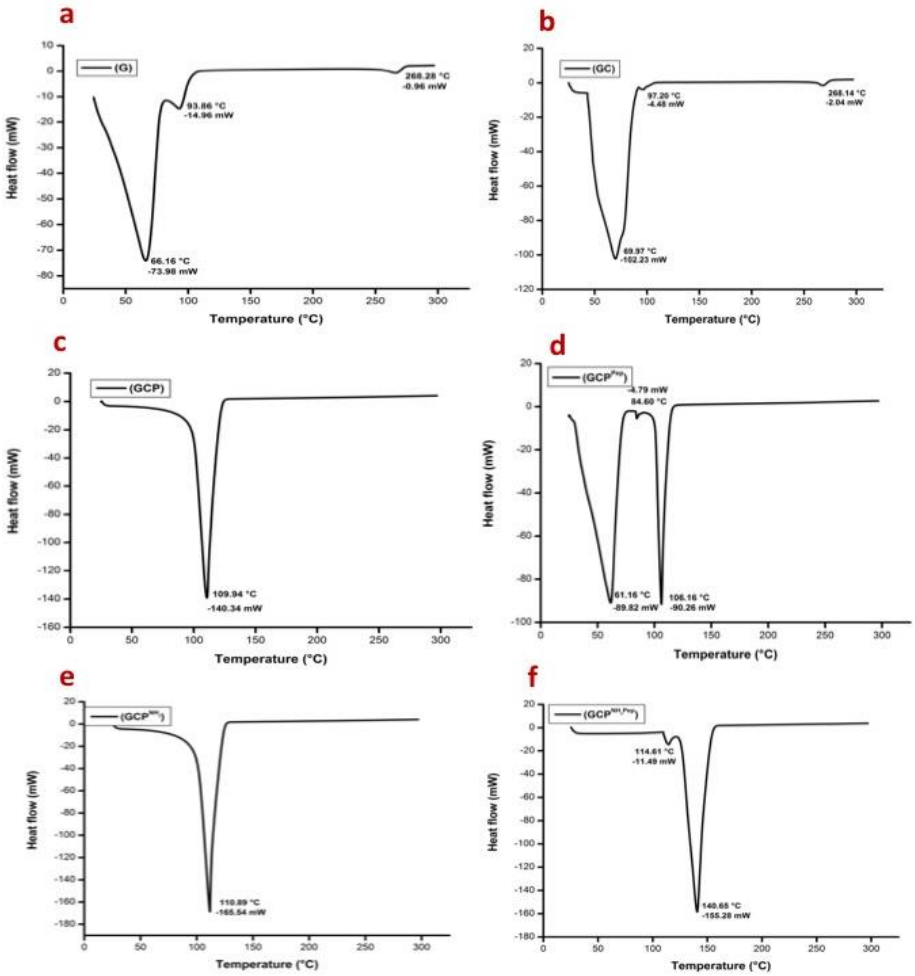

Figure 6. DSC thermogram of synthesized and functionalized rods (**A**) G, (**B**) GC, (**C**) GCP, (**D**) GCP^{Pep}, (**E**) GCP^{NH2}, (**F**) GCP^{NH2Pep}.

An unknown concentration of curcumin was coated on gold nanorods (GC), and the drug release of curcumin from GCP^{Pep} at pH 7.4 and pH 5.5 and from $GCP^{PNH2Pep}$ at pH 7.4 and 5.5 after incubating for 2 hours was determined and found to be 0.1µg, 0.21 µg,0.23 µg, and 0.42 µg respectively. When compared to GCP at 7.4 and 5.5 and GCP^{NH2Pep} at 7.4, there is a one-fold increase in drug released by GCP^{NH2Pep} at pH 5.5, indicating the role of pH-sensitive polymer in drug release. Supplementary information **(**Figure S3**)** provides the chromatograms that show the presence of curcumin and its derivatives with an RT of 5.3, matching closely with RT of 5.36 for a λ max of 424 nm for standard curcumin. The concentration of gold nanoparticles in GCP^{Pep} and GCP^{NH2Pep}, G, GC, GCP, GCP^{NH2} was obtained through ICP-OES analysis. The concentration of gold in the first product, G, was found to be 9.5 µg/mL. The level of gold in the final products GCP^{Pep} was found to be 0.66 µg/mL, and in GCP^{NH2PEP} was found to be 1.33 µg/mL.

3.8. Differential scanning calorimetric analysis.

DSC analysis (Figures 6 a-f) provided information on the thermal stability of G, GC, GCP, and GCP^{NH2Pep}. Two endothermic peaks at 66 and 93°C were characteristic for G, and one peak at 70, 109, and 110°C, respectively, for GC, GCP, and GCP^{NH2}. The increase in temperature is an indication of the increased stability of functionalization. In the case of GCP^{Pep}, three endothermic peaks were observed at 61, 84, and 106°C, indicating that the lower temperature peaks possibly were due to the presence of free gold nanorods or peptides in the system. It has been further confirmed that only two peaks were observed with GCP^{NH2Pep}, of which only one was prominent at 140°C, indicating that the presence of the amino group contributed significantly to the stability of the system.

3.9. Cellular uptake of gold nanorods in PC 12 cells.

By seeding gold nanoparticles to PC 12 cells in Dulbecco's medium, the cellular uptake of gold nanoparticles was determined. For this, 3 µg of G, GC, GCP, GCP^{Pep}, GCP^{NH2}, and GCP^{NH2Pep} is seeded and incubated for 2 h, followed by centrifugation. From the ICP-OES analysis of the supernatant, the percentage of cellular uptake of gold nanorods was determined as 3, 8, 22, 30, 32, 39, and 43%, respectively (Figure 7) for G, GC, GCP, GCP^{Pep}, GCP^{NH2}, and GCP^{NH2pep}. Usually, nanoparticles have potential interactions with living cells (Pengyang et al., 2015), and the negative environment of the extracellular matrix of PC 12 cells and the positively charged nanoparticles have a strong binding to each other. Initially, G is bound to positively charged CTAB; the replacement of CTAB with curcumin leads to GC, and further PEG coating increases the positive charge of the nanoparticle, which increases with NH2-PEG, PLH, and peptide [58]. The results are in tune with reports that are increasing the positive charge of the nanoparticles and increasing the uptake by PC 12 cells [59]. The functionality modifications carried out in this study have only facilitated the increase in the positive charge of the nanoparticles and thus the cellular uptake.

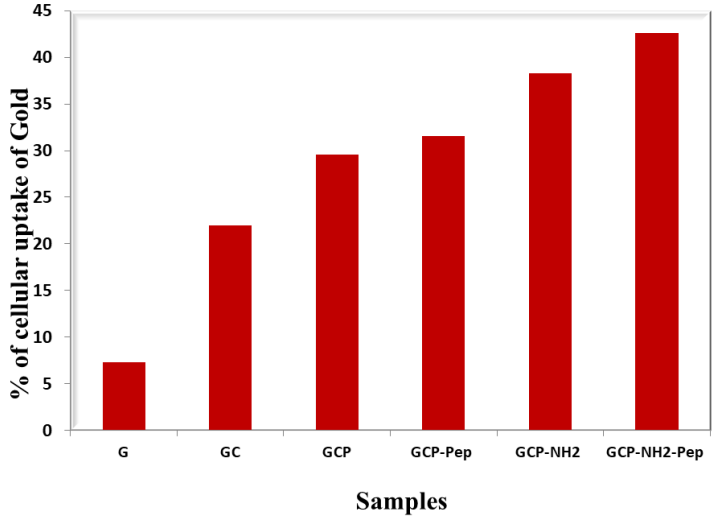

Figure 7. Cellular uptake of synthesized and functionalized gold nanorods.

3.10. HUVEC cells and tube formation assay.

The use of tube formation assays can well study angiogenesis involved in various pathological processes in the body. These have a significant advantage over other tests due to their high throughput screening. We used here human umbilical vein endothelial cells. The tube formation assay [60] was carried out with laminin-1 peptide replaced with gold nanorods and

gold nanorods functionalized with PEG. For this, the 96-well plates were coated with 50 µL of matrigel and incubated at 37°C for 30 min to promote gelling. The angiogenic G or GCPPNH2Pep peptide was added. After 18 h, the plates were fixed with microscopy, and morphology was observed. The presence of a higher concentration of αv β3 integrins in HUVEC cells results in more binding and uptake of ATWLPPR peptide-modified amine-functionalized pH-sensitive polymer gold nanorods. Compared to other samples, GCPNH2Pep shows better inhibition of tube formation in HUVEC cells owing to the significant expression of αv β3 integrins due to their angiogenic phenotype [61]. A clump or cell formation patches were observed in other wells with no peptide samples, as shown in Figure 8.

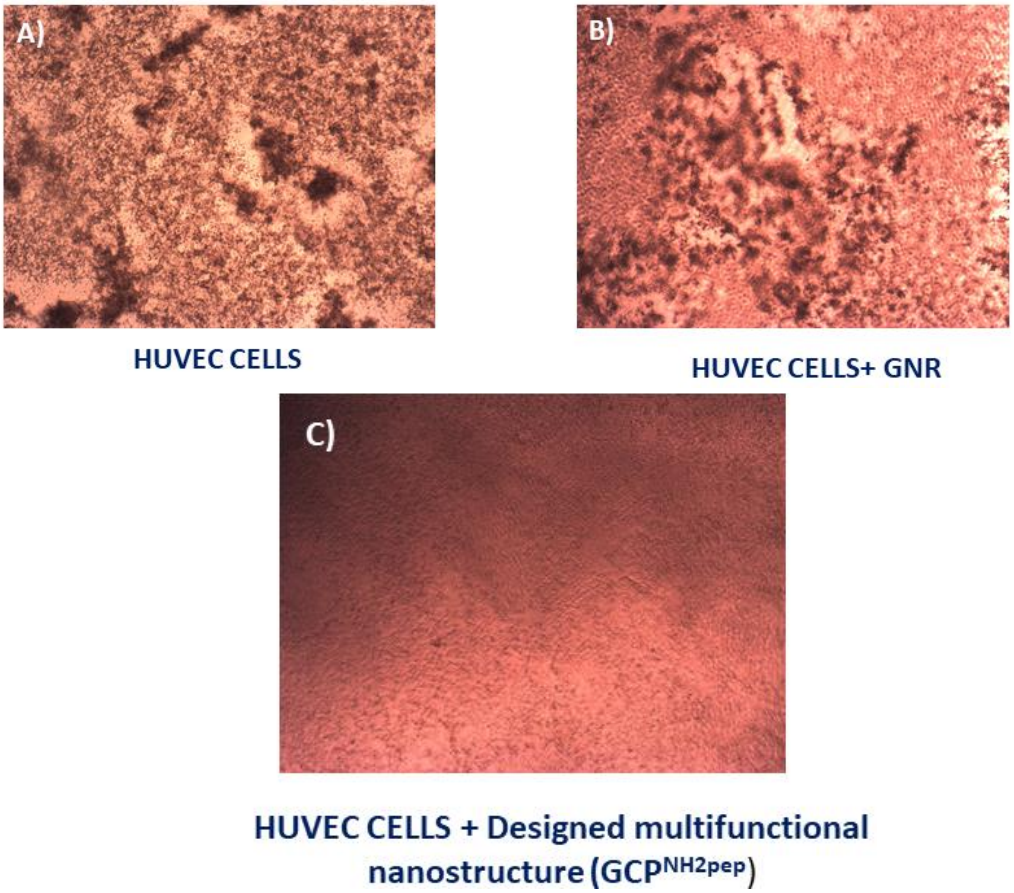

Figure 8. Effect of the functionalized peptide on endothelial tube formation, (**A**) HUVEC cells alone, (**B**) HUVEC cells + GCP, (**C**) HUVEC cells + GCP^{NH2PEP}.

4. Conclusions

One of the proposed advantages of nanotechnology in medicine is the possibility of enhancing the bioavailability of natural product-based drugs, thus reducing side effects due to overdose. Curcumin is an age-old natural product known for its medicinal effects, and the utility has been limited due to its limited solubility in aqueous systems. This work reports the preparation of a nano(drug) carrier, which has curcumin for conventional therapy, gold nanorods for photothermal treatment, the peptide ATWLPPR for targeting NRP-1, and poly(L-histidine) for pH-sensitive release of curcumin. The product had significant thermal stability and carried more curcumin and gold nanoparticles than GC. The cellular uptake of gold nanorods was 43% for GCPNH$_2$Pep as against 8% for the gold-curcumin complex. With tube formation assays as the marker for angiogenesis, our study shows that GCPNH$_2$Pep gave better

inhibition of tube formation. The nano (drug) carrier reported serves as a combination of biotherapeutic and photothermal therapeutic.

Funding

This research received no external funding.

Acknowledgments

This work was supported by the Chettinad Academy of Research and Education, Tamil Nadu, India. We thank CSIR-CLRI for the instrumentation facilities.

Conflicts of Interest

The authors declare no conflict of interest.

References

1. Grewal, I.K.; Singh, S.; Arora, S.; Sharma, N. Polymeric nanoparticles for breast cancer therapy: A comprehensive review. *Biointerface Res. Appl. Chem* **2021**, *11*, 11151-11171, https://doi.org/10.33263/BRIAC114.1115111171.
2. Qorri, B.; DeCarlo, A.; Mellon, M.; Szewczuk, M.R. Chapter 20 - Drug delivery systems in cancer therapy. In *Drug Delivery Devices and Therapeutic Systems*, Chappel, E., Ed.; Academic Press: 2021; pp. 423-454, https://doi.org/10.1016/B978-0-12-819838-4.00016-X.
3. Caballero, D.; Abreu, C.M.; Lima, A.C.; Neves, N.N.; Reis, R.L.; Kundu, S.C. Precision biomaterials in cancer theranostics and modelling. *Biomaterials* **2022**, *280*, 121299, https://doi.org/10.1016/j.biomaterials.2021.121299.
4. Pivetta, T.P.; Botteon, C.E.A.; Ribeiro, P.A.; Marcato, P.D.; Raposo, M. Nanoparticle Systems for Cancer Phototherapy: An Overview. *Nanomaterials* **2021**, *11*, 3132, https://doi.org/10.3390/nano11113132.
5. Moodley, T.; Singh, M. Polymeric mesoporous silica nanoparticles for combination drug delivery in vitro. *Biointerface Res. Appl. Chem* **2020**, *11*, 11905-11919, https://doi.org/10.33263/BRIAC114.1190511919.
6. Cai, W.; Gao, T.; Hong, H.; Sun, J. Applications of gold nanoparticles in cancer nanotechnology. *Nanotechnol Sci Appl* **2008**, *1*, 17-32, https://doi.org/10.2147/NSA.S3788.
7. Hu, X.; Zhang, Y.; Ding, T.; Liu, J.; Zhao, H. Multifunctional Gold Nanoparticles: A Novel Nanomaterial for Various Medical Applications and Biological Activities. *Frontiers in Bioengineering and Biotechnology* **2020**, *8*, https://doi.org/10.3389/fbioe.2020.00990.
8. Khan, N.U.; Lin, J.; Younas, M.R.; Liu, X.; Shen, L. Synthesis of gold nanorods and their performance in the field of cancer cell imaging and photothermal therapy. *Cancer Nanotechnology* **2021**, *12*, 20, https://doi.org/10.1186/s12645-021-00092-w.
9. Zhao, S.; Luo, Y.; Chang, Z.; Liu, C.; Li, T.; Gan, L.; Huang, Y.; Sun, Q. BSA-Coated Gold Nanorods for NIR-II Photothermal Therapy. *Nanoscale Research Letters* **2021**, *16*, 170, https://doi.org/10.1186/s11671-021-03627-7.
10. Bansal, S.A.; Kumar, V.; Karimi, J.; Singh, A.P.; Kumar, S. Role of gold nanoparticles in advanced biomedical applications. *Nanoscale Advances* **2020**, *2*, 3764-3787, https://doi.org/10.1039/D0NA00472C.
11. Joshi, P.; Joshi, S.; Semwal, D.; Bisht, A.; Paliwal, S.; Dwivedi, J.; Sharma, S. Curcumin: An Insight into Molecular Pathways Involved in Anticancer Activity. *Mini reviews in medicinal chemistry* **2021**, *21*, 2420-2457, https://doi.org/10.2174/1389557521666210122153823.
12. Sharifi-Rad, J.; Rayess, Y.E.; Rizk, A.A.; Sadaka, C.; Zgheib, R.; Zam, W.; Sestito, S.; Rapposelli, S.; Neffe-Skocińska, K.; Zielińska, D.; Salehi, B.; Setzer, W.N.; Dosoky, N.S.; Taheri, Y.; El Beyrouthy, M.; Martorell, M.; Ostrander, E.A.; Suleria, H.A.R.; Cho, W.C.; Maroyi, A.; Martins, N. Turmeric and Its Major Compound Curcumin on Health: Bioactive Effects and Safety Profiles for Food, Pharmaceutical, Biotechnological and Medicinal Applications. *Front Pharmacol* **2020**, *11*, 01021-01021, https://doi.org/10.3389/fphar.2020.01021.
13. Jurenka, J.S. Anti-inflammatory properties of curcumin, a major constituent of Curcuma longa: a review of preclinical and clinical research. *Alternative medicine review : a journal of clinical therapeutic* **2009**, *14*, 141-153.

14. Sultana, S.; Munir, N.; Mahmood, Z.; Riaz, M.; Akram, M.; Rebezov, M.; Kuderinova, N.; Moldabayeva, Z.; Shariati, M.A.; Rauf, A.; rengasamy, K.R.R. Molecular targets for the management of cancer using Curcuma longa Linn. phytoconstituents: A Review. *Biomedicine & Pharmacotherapy* **2021**, *135*, 111078, https://doi.org/10.1016/j.biopha.2020.111078.
15. Zheng, B.; McClements, D.J. Formulation of More Efficacious Curcumin Delivery Systems Using Colloid Science: Enhanced Solubility, Stability, and Bioavailability. *Molecules* **2020**, *25*, 2791, https://doi.org/10.3390/molecules25122791.
16. Wu, J. The Enhanced Permeability and Retention (EPR) Effect: The Significance of the Concept and Methods to Enhance Its Application. *J Pers Med* **2021**, *11*, 771, https://doi.org/10.3390/jpm11080771.
17. Shi, L.; Zhang, J.; Zhao, M.; Tang, S.; Cheng, X.; Zhang, W.; Li, W.; Liu, X.; Peng, H.; Wang, Q. Effects of polyethylene glycol on the surface of nanoparticles for targeted drug delivery. *Nanoscale* **2021**, *13*, 10748-10764, https://doi.org/10.1039/D1NR02065J.
18. Mitchell, M.J.; Billingsley, M.M.; Haley, R.M.; Wechsler, M.E.; Peppas, N.A.; Langer, R. Engineering precision nanoparticles for drug delivery. *Nature Reviews Drug Discovery* **2021**, *20*, 101-124, https://doi.org/10.1038/s41573-020-0090-8.
19. Ofridam, F.; Tarhini, M.; Lebaz, N.; Gagnière, É.; Mangin, D.; Elaissari, A. pH-sensitive polymers: Classification and some fine potential applications. *Polymers for Advanced Technologies* **2021**, *32*, 1455-1484, https://doi.org/10.1002/pat.5230.
20. Xie, L.; Liu, R.; Chen, X.; He, M.; Zhang, Y.; Chen, S. Micelles Based on Lysine, Histidine, or Arginine: Designing Structures for Enhanced Drug Delivery. *Frontiers in Bioengineering and Biotechnology* **2021**, *9*, https://doi.org/10.3389/fbioe.2021.744657.
21. Peng, K.; Bai, Y.; Zhu, Q.; Hu, B.; Xu, Y. Targeting VEGF–neuropilin interactions: a promising antitumor strategy. *Drug Discovery Today* **2019**, *24*, 656-664, doi:https://doi.org/10.1016/j.drudis.2018.10.004.
22. Liu, S.-D.; Zhong, L.-P.; He, J.; Zhao, Y.-X. Targeting neuropilin-1 interactions is a promising anti-tumor strategy. *Chin Med J (Engl)* **2021**, *134*, 508-517, https://doi.org/10.1097/CM9.0000000000001200.
23. Dhaini, B.; Kenzhebayeva, B.; Ben-Mihoub, A.; Gries, M.; Acherar, S.; Baros, F.; Thomas, N.; Daouk, J.; Schohn, H.; Hamieh, T.;Frochot, C. Peptide-conjugated nanoparticles for targeted photodynamic therapy. *Nanophotonics* **2021**, *10*, 3089-3134, https://doi.org/10.1515/nanoph-2021-0275.
24. Sheikh, A.; Alhakamy, N.A.; Md, S.; Kesharwani, P. Recent Progress of RGD Modified Liposomes as Multistage Rocket Against Cancer. *Front Pharmacol* **2022**, *12*, https://doi.org/10.3389/fphar.2021.803304.
25. Wilken, R.; Veena, M.S.; Wang, M.B.; Srivatsan, E.S. Curcumin: A review of anticancer properties and therapeutic activity in head and neck squamous cell carcinoma. *Molecular Cancer* **2011**, *10*, 12-12, https://doi.org/10.1186/1476-4598-10-12.
26. Sau, T.K.; Murphy, C.J. Seeded high yield synthesis of short Au nanorods in aqueous solution. *Langmuir : the ACS journal of surfaces and colloids* **2004**, *20*, 6414-6420, https://doi.org/10.1021/la049463z.
27. Singh, D.K.; Jagannathan, R.; Khandelwal, P.; Abraham, P.M.; Poddar, P. In situ synthesis and surface functionalization of gold nanoparticles with curcumin and their antioxidant properties: an experimental and density functional theory investigation. *Nanoscale* **2013**, *5*, 1882-1893, https://doi.org/10.1039/C2NR33776B.
28. Sindhu, K.; Rajaram, A.; Sreeram, K.J.; Rajaram, R. Curcumin conjugated gold nanoparticle synthesis and its biocompatibility. *RSC Adv* **2014**, *4*, 1808-1818, https://doi.org/10.1039/C3RA45345F.
29. Qin, W.; Huang, G.; Chen, Z.; Zhang, Y. Nanomaterials in Targeting Cancer Stem Cells for Cancer Therapy. *Front Pharmacol* **2017**, *8*, 1, https://doi.org/10.3389/fphar.2017.00001.
30. Seol, S.K.; Kim, D.; Jung, S.; Chang, W.S.; Kim, J.T. One-Step Synthesis of PEG-Coated Gold Nanoparticles by Rapid Microwave Heating. *J Nanomater* **2013**, *2013*, 6, https://doi.org/10.1155/2013/531760.
31. Starzec, A.; Ladam, P.; Vassy, R.; Badache, S.; Bouchemal, N.; Navaza, A.; du Penhoat, C.H.; Perret, G.Y. Structure-function analysis of the antiangiogenic ATWLPPR peptide inhibiting VEGF(165) binding to neuropilin-1 and molecular dynamics simulations of the ATWLPPR/neuropilin-1 complex. *Peptides* **2007**, *28*, 2397-2402, https://doi.org/10.1016/j.peptides.2007.09.013.
32. Roberts, M.J.; Bentley, M.D.; Harris, J.M. Chemistry for peptide and protein PEGylation. *Advanced drug delivery reviews* **2002**, *54*, 459-476, https://doi.org/10.1016/s0169-409x(02)00022-4.
33. Bilalis, P.; Tziveleka, L.-A.; Varlas, S.; Iatrou, H. pH-Sensitive nanogates based on poly(l-histidine) for controlled drug release from mesoporous silica nanoparticles. *Polym Chem* **2016**, *7*, 1475-1485, https://doi.org/10.1039/C5PY01841B.
34. Liu, Y.; Feng, L.; Liu, T.; Zhang, L.; Yao, Y.; Yu, D.; Wang, L.; Zhang, N.. Multifunctional pH-sensitive polymeric nanoparticles for theranostics evaluated experimentally in cancer. *Nanoscale* **2014**, *6*, 3231-3242, https://doi.org/10.1039/C3NR05647C.

35. Zhang, J.; Liu, X.; Yu, W.; Zhang, Y.; Shi, C.; Ni, S.; Liu, Q.; Li, X.; Sun, Y.; Zheng, C.; Sun, H. Effects of human vascular endothelial growth factor on reparative dentin formation. *Molecular medicine reports* **2016**, *13*, 705-712, https://doi.org/10.3892/mmr.2015.4608.
36. Martin, R.C.; Locatelli, E.; Li, Y.; Zhang, W.; Li, S.; Monaco, I.; Franchini, M.C. Gold nanorods and curcumin-loaded nanomicelles for efficient in vivo photothermal therapy of Barrett's esophagus. *Nanomedicine (London, England)* **2015**, *10*, 1723-1733, https://doi.org/10.2217/nnm.15.25.
37. Plowman, B.J.; Tschulik, K.; Young, N.P.; Compton, R.G. Capping agent promoted oxidation of gold nanoparticles: cetyl trimethylammonium bromide. *Phys Chem Chem Phys* **2015**, *17*, 26054-26058, https://doi.org/10.1039/C5CP05146K.
38. Scarabelli, L.; Sánchez-Iglesias, A.; Pérez-Juste, J.; Liz-Marzán, L.M. A "Tips and Tricks" Practical Guide to the Synthesis of Gold Nanorods. *J Phys Chem Lett* **2015**, *6*, 4270-4279, https://doi.org/10.1021/acs.jpclett.5b02123.
39. Durr, N.J.; Larson, T.; Smith, D.K.; Korgel, B.A.; Sokolov, K.; Ben-Yakar, A. Two-Photon Luminescence Imaging of Cancer Cells using Molecularly Targeted Gold Nanorods. *Nano lett* **2007**, *7*, 941-945, https://doi.org/10.1021/nl062962v.
40. Xu, X.; Zhao, Y.; Xue, X.; Huo, S.; Chen, F.; Zou, G.; Liang, X.-J. Seedless synthesis of high aspect ratio gold nanorods with high yield. *J Mater Chem A* **2014**, *2*, 3528-3535, https://doi.org/10.1039/C3TA13905K.
41. Koeppl, S.; Solenthaler, C.; Caseri, W.; Spolenak, R. Towards a Reproducible Synthesis of High Aspect Ratio Gold Nanorods. *J Nanomater* **2011**, *2011*, 13.
42. Zhang, G.; Yang, Z.; Lu, W.; Zhang, R.; Huang, Q.; Tian, M.; Li, L.; Liang, D.; Li, C.. Influence of anchoring ligands and particle size on the colloidal stability and in vivo biodistribution of polyethylene glycol-coated gold nanoparticles in tumor-xenografted mice. *Biomaterials* **2009**, *30*, 1928-1936, https://doi.org/10.1016/j.biomaterials.2008.12.038.
43. Teesalu, T.; Sugahara, K.N.; Kotamraju, V.R.; Ruoslahti, E. C-end rule peptides mediate neuropilin-1-dependent cell, vascular, and tissue penetration. *Proc Natl Acad Sci U S A* **2009**, *106*, 16157-16162, https://doi.org/10.1073/pnas.0908201106.
44. Chen, H.; Zhang, X.; Dai, S.; Ma, Y.; Cui, S.; Achilefu, S.; Gu, Y. Multifunctional Gold Nanostar Conjugates for Tumor Imaging and Combined Photothermal and Chemo-therapy. *Theranostics* **2013**, *3*, 633-649, https://doi.org/10.7150/thno.6630.
45. Taheri, R.A.; Akhtari, Y.; Tohidi Moghadam, T.; Ranjbar, B. Assembly of Gold Nanorods on HSA Amyloid Fibrils to Develop a Conductive Nanoscaffold for Potential Biomedical and Biosensing Applications. *Scientific Reports* **2018**, *8*, 9333, https://doi.org/10.1038/s41598-018-26393-6.
46. Wang, J.; Dong, B.; Chen, B.; Jiang, Z.; Song, H. Selective photothermal therapy for breast cancer with targeting peptide modified gold nanorods. *Dalton Transactions* **2012**, *41*, 11134-11144, https://doi.org/10.1039/C2DT31227A.
47. Sun, T.-W.; Zhu, Y.-J.; Chen, F. Hydroxyapatite nanowire/collagen elastic porous nanocomposite and its enhanced performance in bone defect repair. *RSC Advances* **2018**, *8*, 26218-26229, https://doi.org/10.1039/C8RA03972K.
48. Siafaka, P.; Üstündağ Okur, N.; Karavas, E.; Bikiaris, D. Surface Modified Multifunctional and Stimuli Responsive Nanoparticles for Drug Targeting: Current Status and Uses. *Int J Mol Sci* **2016**, *17*, 1440, https://doi.org/10.3390/ijms17091440.
49. Nel, A.E.; Madler, L.; Velegol, D.; Xia, T.; Hoek, E.M.V.; Somasundaran, P.; Klaessig, F.; Castranova, V.; Thompson, M.. Understanding biophysicochemical interactions at the nano-bio interface. *Nat Mater* **2009**, *8*, 543-557, https://doi.org/10.1038/nmat2442.
50. Min, Y.; Akbulut, M.; Kristiansen, K.; Golan, Y.; Israelachvili, J. The role of interparticle and external forces in nanoparticle assembly. *Nat Mater* **2008**, *7*, 527-538, https://doi.org/10.1038/nmat2206.
51. Fosgerau, K.; Hoffmann, T. Peptide therapeutics: current status and future directions. *Drug Discov Today* **2015**, *20*, 122-128, https://doi.org/10.1016/j.drudis.2014.10.003.
52. Lombardo, D.; Calandra, P.; Barreca, D.; Magazù, S.; Kiselev, M.A. Soft Interaction in Liposome Nanocarriers for Therapeutic Drug Delivery. *Nanomaterials* **2016**, *6*, 125, https://doi.org/10.3390/nano6070125.
53. Li, T.; Shen, X.; Chen, Y.; Zhang, C.; Yan, J.; Yang, H.; *et . al.* Polyetherimide-grafted Fe(3)O(4)@SiO2(2) nanoparticles as theranostic agents for simultaneous VEGF siRNA delivery and magnetic resonance cell imaging. *International journal of nanomedicine* **2015**, *10*, 4279-4291, https://doi.org/10.2147/IJN.S85095.
54. Zhang, B.; Yan, B. Analytical Strategies for Characterizing Nanoparticle's Surface Chemistry. *Anal Bioanal Chem* **2010**, *396*, 973, https://doi.org/10.1007/s00216-009-2996-1.
55. Zhu, Z. Effects of amphiphilic diblock copolymer on drug nanoparticle formation and stability. *Biomaterials* **2013**, *34*, 10238-10248, https://doi.org/10.1016/j.biomaterials.2013.09.015.

56. Ghosh, M.; Singh, A.T.K.; Xu, W.; Sulchek, T.; Gordon, L.I.; Ryan, R.O. Curcumin nanodisks: formulation and characterization. *Nanomed Nanotech Biol Med* **2011**, *7*, 162-167, https://doi.org/10.1016/j.nano.2010.08.002.
57. Ang, L.F.; Yam, M.F.; Fung, Y.T.T.; Kiang, P.K.; Darwin, Y. HPLC Method for Simultaneous Quantitative Detection of Quercetin and Curcuminoids in Traditional Chinese Medicines. *J Pharmacopuncture* **2014**, *17*, 36-49, https://doi.org/10.3831/KPI.2014.17.035.
58. Freese, C.; Anspach, L.; Deller, R.C.; Richards, S.J.; Gibson, M.I.; Kirkpatrick, C.J.; Unger, R.E. Gold nanoparticle interactions with endothelial cells cultured under physiological conditions. *Biomaterials science* **2017**, *5*, 707-717, https://doi.org/10.1039/C6BM00853D.
59. Frohlich, E. The role of surface charge in cellular uptake and cytotoxicity of medical nanoparticles. *International journal of nanomedicine* **2012**, *7*, 5577-5591, https://doi.org/10.2147/IJN.S36111.
60. Malinda, K.M.; Nomizu, M.; Chung, M.; Delgado, M.; Kuratomi, Y.; Yamada, Y.; Kleinman, H.K.; Ponce, M.L. Identification of laminin alpha1 and beta1 chain peptides active for endothelial cell adhesion, tube formation, and aortic sprouting. *FASEB journal : official publication of the Federation of American Societies for Experimental Biology* **1999**, *13*, 53-62.
61. Weis, S.M.; Cheresh, D.A. αV integrins in angiogenesis and cancer. *Cold Spring Harb Perspect Med* **2011**, *1*, a006478-a006478, https://doi.org/10.1101/cshperspect.a006478.

Supplementary information

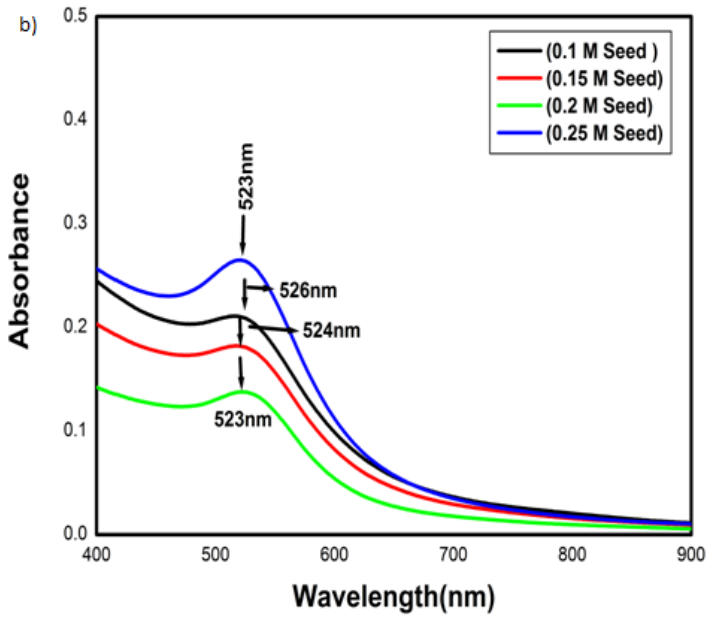

Figure S1. The seed solution with different concentrations of CTAB.

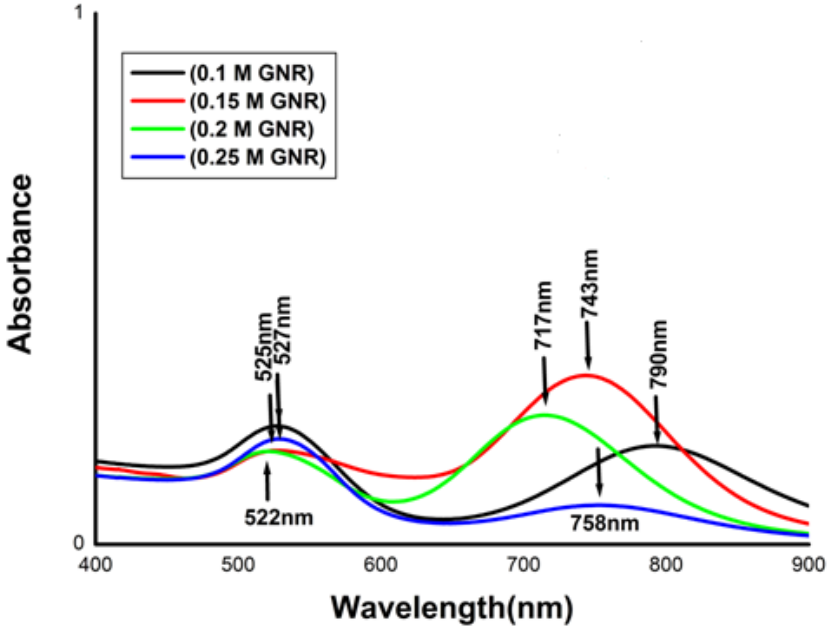

Figure S2. The G solutions with varying levels of seed solutions.

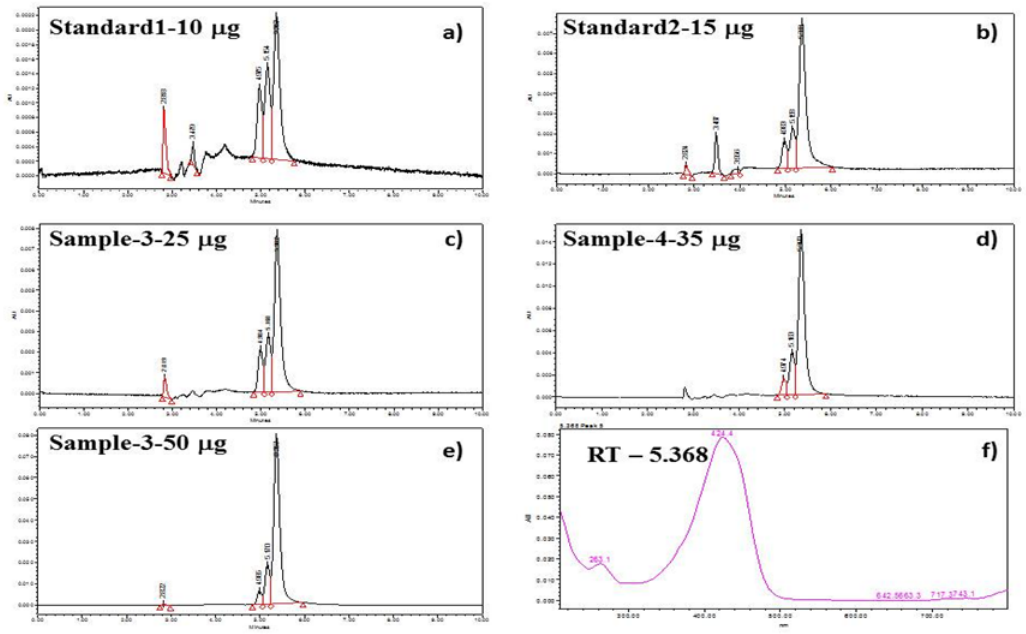

Standard HPLC chromatogram

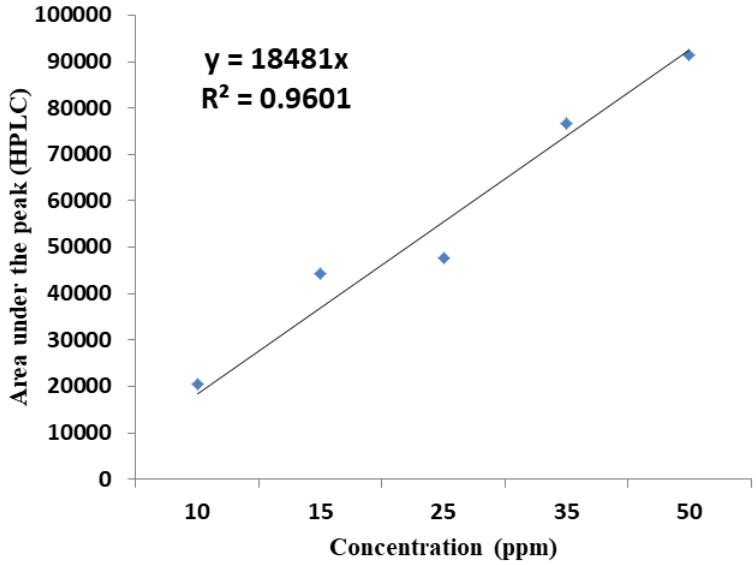

Figure S3. Chromatograms shows the presence of curcumin and its derivatives.